AGU PUBLICATIONS

Geophysical Research Letters

RESEARCH LETTER
10.1002/2016GL069204

Key Points:
- Warm Water Volume and wind stress forcing throughout the boreal spring and summer are both needed for an El Niño event
- The easterly wind burst in July 2014 created conditions favorable for the development of the 2015-2016 El Niño event
- Wind stress forcing through the boreal summer can have an impact on El Niño 18 months later by influencing warm water volume anomaly

Supporting Information:
- Supporting Information S1

Correspondence to:
A. F. Z. Levine,
aaron.levine@noaa.gov

Citation:
Levine, A. F. Z., and M. J. McPhaden (2016), How the July 2014 easterly wind burst gave the 2015-2016 El Niño a head start, *Geophys. Res. Lett.*, *43*, 6503–6510, doi:10.1002/2016GL069204.

Received 8 MAR 2016
Accepted 22 APR 2016
Accepted article online 26 APR 2016
Published online 24 JUN 2016

How the July 2014 easterly wind burst gave the 2015–2016 El Niño a head start

Aaron F. Z. Levine[1] and Michael J. McPhaden[1]

[1] NOAA/PMEL, Seattle, Washington, USA

Abstract Following strong westerly wind bursts in boreal winter and spring of 2014, both the scientific community and the popular press were abuzz with the possibility of a major El Niño developing. However, during the boreal summer of 2014, the Bjerknes feedback failed to kick in, aided and abetted by a strong easterly wind burst. The widely anticipated major 2014–2015 El Niño event failed to materialize and even failed to qualify as an El Niño by conventional definitions. However, the boreal summer easterly wind burst had the effect of not only inhibiting the growth of the El Niño event but also preventing and then reversing the discharge of the equatorial heat content that typically occurs during the course of an El Niño event. This head start of equatorial heat content helped push the 2015–2016 El Niño event to extreme magnitude.

1. Introduction

In theoretical descriptions of El Niño–Southern Oscillation (ENSO), wind stress forcing has a large role determining the size and timing of events [*Penland*, 1996; *Penland and Sardeshmukh*, 1995]. This forcing is characterized by westerly wind bursts (WWBs) which force eastward current that advect the western Pacific warm pool into the central Pacific and excite downwelling Kelvin waves along the thermocline across the equatorial Pacific [*McPhaden et al.*, 1988]. Typically, more than one WWB is needed to trigger an El Niño event and the largest events are initiated by multiple WWBs that occur throughout the growth phase of the El Niño event [*McPhaden*, 1999; *Yu et al.*, 2003]. Additional WWBs become more likely after the first WWB through a process known as state-dependent noise forcing [*Eisenman et al.*, 2005; *Jin et al.*, 2007; *Levine and Jin*, 2010, 2015]. Given what is currently known about WWBs and El Niño, the large WWBs in spring of 2014 and accompanying downwelling Kelvin waves captured the attention of the scientific community. The excitement this generated was picked up on by the media with many stories reporting on the likelihood of an extreme El Niño event to peak in the winter of 2014–2015 [*McPhaden*, 2015]. However, during the summer of 2014, instead of continued WWBs, a large easterly wind burst (EWB) occurred. This EWB halted the development of the El Niño event leading to borderline El Niño conditions that occurred during the winter of 2014–2015 [*Menkes et al.*, 2014; *Hu and Fedorov*, 2016]. As we will show in this paper, this false start in 2014 gave a head start to the extreme El Niño event of 2015–2016 (http://www.cpc.ncep.noaa.gov/products/analysis_monitoring/enso_disc_dec2015/ensodisc.html).

Beyond wind stress forcing of ENSO, another traditionally necessary but not sufficient condition is a buildup of anomalous warm water volume (WWV) over the upper part of the tropical Pacific Ocean [*Wyrtki*, 1985; *Jin*, 1997; *Meinen and McPhaden*, 2000]. The WWV builds up and acts as a reservoir of heat that fuels development during the El Niño event typically leading the surface warming by 6–9 months [*McPhaden*, 2002; *Yu and Kao*, 2007; *McPhaden*, 2012]. In recharge oscillator theory, this excess heat content is discharged poleward by the anomalous westerly winds that accompany an El Niño event [*Jin*, 1997]. The discharge of heat content acts as the delayed negative feedback that terminates the El Niño and sets the stage for a possible follow-on La Niña event. Given the role of the EWB in halting the development of the El Niño event in 2014, the question of how that EWB affected the anomalous WWV in the equatorial Pacific also needs to be explored. In this paper, we utilize the recharge/discharge paradigm, examining the changes in winds, WWV, and sea surface temperature (SST) during 2014–2016. We will show that the EWB that halted the 2014-5 El Niño growth also gave a head start to the extreme El Niño of 2015–2016. This false start/head start mechanism has occurred before in instrumental record. Additionally, we will show that when a developing El Niño event is halted in the boreal summer by an EWB, the ENSO system has a modest amount of additional predictability at lead times of one and a half years.

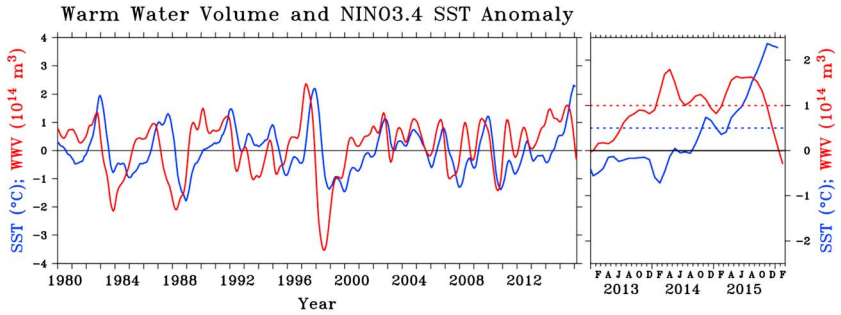

Figure 1. Time series of WWV and Nino3.4 from 1980-present using ERSSTv4. (left) Five month running means. (right) Monthly means since 2013, with the dashed blue line being the 0.5°C threshold for El Niño events and the dashed red line being 1×10^{14} m^3, a WWV threshold for the development of El Niño events.

2. Data and Methods

For WWV we use WWV from Tropical Atmosphere Ocean/Pacific Marine Environmental Laboratory (PMEL), which are published online at http://www.pmel.noaa.gov/tao/elnino/wwv/data/. This quantity was calculated by averaging the anomalous volume of water above the 20°C isotherm over the region of 120°E–80°W and 5°S–5°N. The ocean analysis used to create these averages is from the Bureau National Operations Centre at the Australian Bureau of Meteorology [*Smith*, 1995]. We use the ERSSTv4 SST product over the Nino3.4 box (120°W–170°W, 5°S–5°N). From their data, a 3 month average Oceanic Niño Index (ONI) can be derived, which is available from NOAA Climate Prediction Center and published online at http://www.cpc.ncep.noaa.gov/products/analysis_monitoring/ensostuff/ensoyears.shtml. The wind stress data is from Global Ocean Data Assimilation System (GODAS) [*Ji et al.*, 1995]. The results are independent of data set for wind stress; we repeat the wind stress plots using TropFlux [*Kumar et al.*, 2012] in the supporting information. All data cover the time period from 1980 to present. Following *Levine and Jin* [2015], to isolate the stochastic component of wind stress forcing from the wind stress response to SST (the so-called Bjerknes feedback), we remove the linear and nonlinear SST feedbacks and annual and semiannual combination tones [*Stuecker et al.*, 2013].

$$\tau_R = \tau_a - \mu_1 T + \mu_2 H(T) T + \mu_{AC} T \sin\left(\omega_{AC} t - t_{AC}\right) + \mu_{SAC} T \sin\left(2\omega_{AC} t - t_{SAC}\right) \quad (1)$$

where τ is the wind stress, T is SST, μ are coupling coefficients, H is a heaviside function, ω_{AC} is the annual cycle frequency, and t_{AC} and t_{SAC} are the combination tone offset from the annual cycle. The coupling coefficients are found using a modified multiple linear regression method. The full details of this method can be found in *Levine and Jin* [2015]. Positive values of τ_R represent anomalous westerly wind stress forcing and negative values easterly wind stress forcing.

3. The Roles of WWV and Wind Stress Forcing for an El Niño Event

Here we examine the two main precursors for El Niño events, WWV, and wind stress forcing. A positive WWV anomaly preconditions the system for an El Niño event and the wind stress forcing helps to initiate the event. WWV tends to lead El Niño SST anomalies by 6–9 months, with El Niño SSTs typically peaking in the boreal winter (Figure 1). We examine the WWV anomaly averaged over February, March, and April (FMA) as a predictor of the eventual El Niño strength. We also compare that with wind stress forcing supplied to the system summed over the months of March through October (Figure 2). This reveals that elevated WWV and wind stress forcing affect the evolution of El Niño events and that for the extreme El Niño events as observed in 1982, 1997, and 2015, both strong wind stress forcing and WWV anomaly are critical. There are two more years in Figure 2 that stand out. Both 1990 and 2014 have extremely large WWV anomalies in FMA but neither has a large sum of wind stress forcing over the following summer and fall. In both cases, the resulting SST anomalies in winter are near the threshold for the definition of what constitutes an El Niño event, defined as five consecutive months with an ONI exceeding 0.5°C. However, in both cases an El Niño event T is SST, occurred the following year. Supporting information Figure S2 confirms that the WWV in FMA of 1990 and 2014 is unusually large, ranking second and third since in WWV anomaly since 1980.

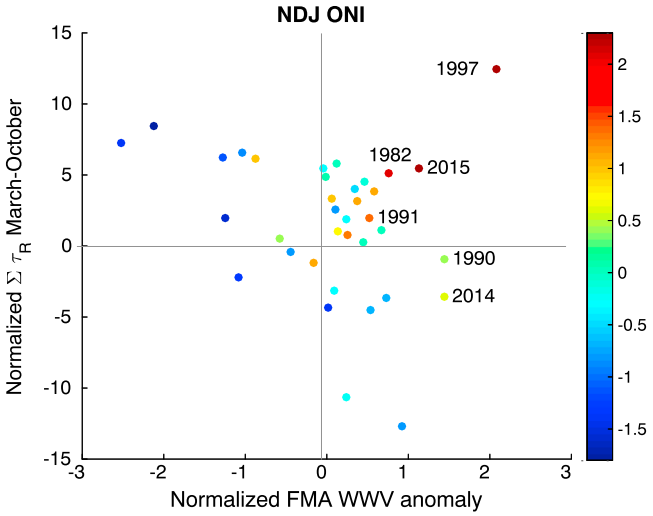

Figure 2. Scatterplot of the February, March, and April (FMA) averaged warm water volume anomaly (WWV) and noise forcing from March to October, both normalized by their respective standard deviations, with the November, December, and January Oceanic Niño Index shown by the colors. El Niño events typically require to both WWV and noise forcing. The largest events have significant amounts of both noise wind forcing and precursory WWV build up. Years 1990 and 2014 stand out for the WWV anomaly without noise forcing, which leads to slightly warm November–January Oceanic Niño Index (ONI) values.

Both the current state of the ocean-atmosphere system and the time of year are important to understand how the wind stress forcing affects the WWV [*Fedorov et al.*, 2014]. In 1990 and 2014, WWBs occurred west of the dateline in the boreal winter (supporting information Figure S3). These WWBs contributed to the buildup of WWV. However, WWBs did not occur during the boreal spring or summer, rather an EWB occurred then. This is drastically different than what happens during a typical El Niño year when WWBs occur through the boreal spring and summer (Figure 3a). No matter the method of detecting EWBs used, no El Niño year in this period has had the same combination of the magnitude and duration of EWBs as compared with 1990 and 2014 [*Hu et al.*, 2014] (supporting information Figures S5–S8). An EWB of this magnitude not only fails to continue forcing the incipient El Niño event but also can counteract the development of the event through westward zonal advection of cold SSTs and an increase in upwelling of cold water in the eastern and central Pacific.

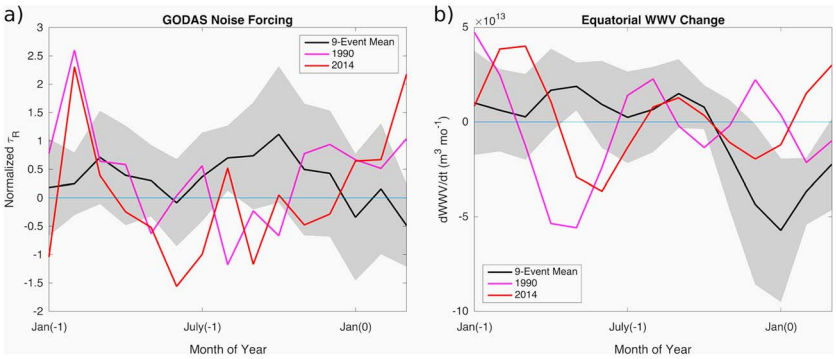

Figure 3. (a) Time series of the monthly mean noise forcing for the nine El Niño events from 1980 to 2012 compared with 1990 and 2014. The shaded area represents $\pm 1\sigma$ from the mean for these nine events. Both 1990 and 2014 have large WWBs in the boreal winter but unlike most other events have strong EWBs during the boreal summer. (b) Time series of $\frac{dWWV}{dt}$ for the nine El Niño events from 1980 to 2012 compared with 1990 and 2014. The shaded area represents $\pm 1\sigma$ from the mean for these nine events. Both 1990 and 2014 show strong discharge (negative values of dWWV/dt) during the boreal spring and then switch to recharge during the boreal summer and fall.

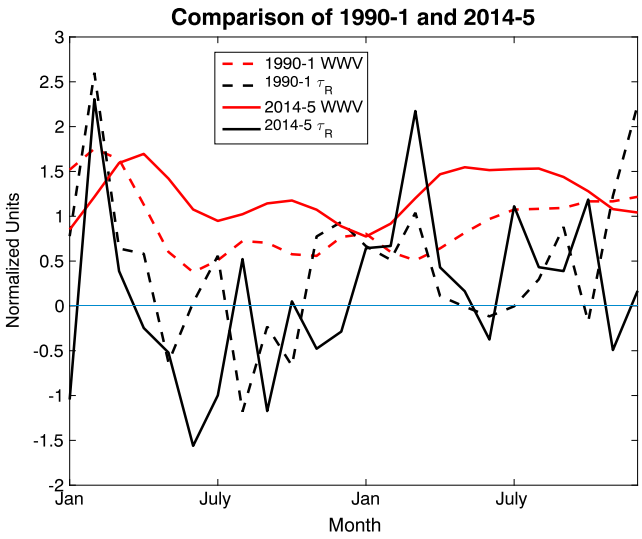

Figure 4. Time series of the WWV and τ_R for 2014-2015 and 1990-1991. Both years end with El Niño events: the event in 2015 is much larger than in 1991, in part due to the much larger noise forcing, τ_R, in 2015 compared with 1991.

4. Applying the Recharge/Discharge Paradigm

The recharge/discharge paradigm for WWV has been successfully applied to the WWV of El Niño events [*Meinen and McPhaden*, 2000; *Ren and Jin*, 2013]. The key to the discharge of equatorial heat content (i.e., negative values of dWWV/dt) is the anomalous westerly winds and associated wind stress curls driving anomalous poleward flow. Supporting information Figure S4 shows that the divergent geostrophic poleward flow from 120°E to 80°W at 5°N and 5°S over the course of the year leading up to the peak of an event is directly proportional to the anomalous wind stress over the El Niño growth period. We can also see that the geostrophic flow in any given month is directly proportional to the rate of change of WWV as we expect if changes in mass and heat content are related to changes in thermocline depth (supporting information Figure S9). The lack of a westerly wind stress anomaly in 1990 and 2014 should then correspond with a lack of heat discharge from the equatorial region, which we see particularly evident in the decreasing total discharge for the boreal summer in 1990 and 2014 (Figure 3b). In particular, the heat content actually increases following the EWBs of the boreal summer in 1990 and 2014 (supporting information Figure S10). The recent finding of *McGregor et al.* [2015] explains how WWBs along the equator can lead to discharge of equatorial heat content several months later. Since EWBs are meridionally broad enough to force the equatorial wave guide [*Hu and Fedorov*, 2016] and the dynamics are linear, so our finding of recharging of the equatorial heat content through an EWB is in agreement with *McGregor et al.* [2015]. We find that the WWV anomaly created early in 1990 and 2014 remains large through the end of and into the next calendar year without dissipating. This is particularly true for 2015 as we find that the FMA WWV in 2015 is the fourth highest in the sample period (supporting information Figure S2).

This heat content that remains because of the false start El Niño events in 1990 and 2014 gives a head start to the El Niño events of 1991 and 2015. Both 1991 and 2015 start with significant heat content anomalies (Figure 4). However, 2015 became an extreme El Niño event, while 1991 was a normal El Niño event. The initial WWBs in 2015 were much stronger and more numerous than those that occurred in 1991. As a result, the WWV anomaly in 2015 grew significantly from its already warm start, while the 1991 WWV anomaly grew only modestly. The WWBs that followed throughout 2015 were also generally larger than those observed throughout 1991, consistent with a stronger El Niño event in 2015 than 1991. Another difference between 1991 and 2015 is the basin-wide warming that was present in 2015 but not in 1991 (supporting information Figure S12). This warming favored more energetic and frequent WWBs, as would be expected for state-dependent noise forcing [*McPhaden*, 2015].

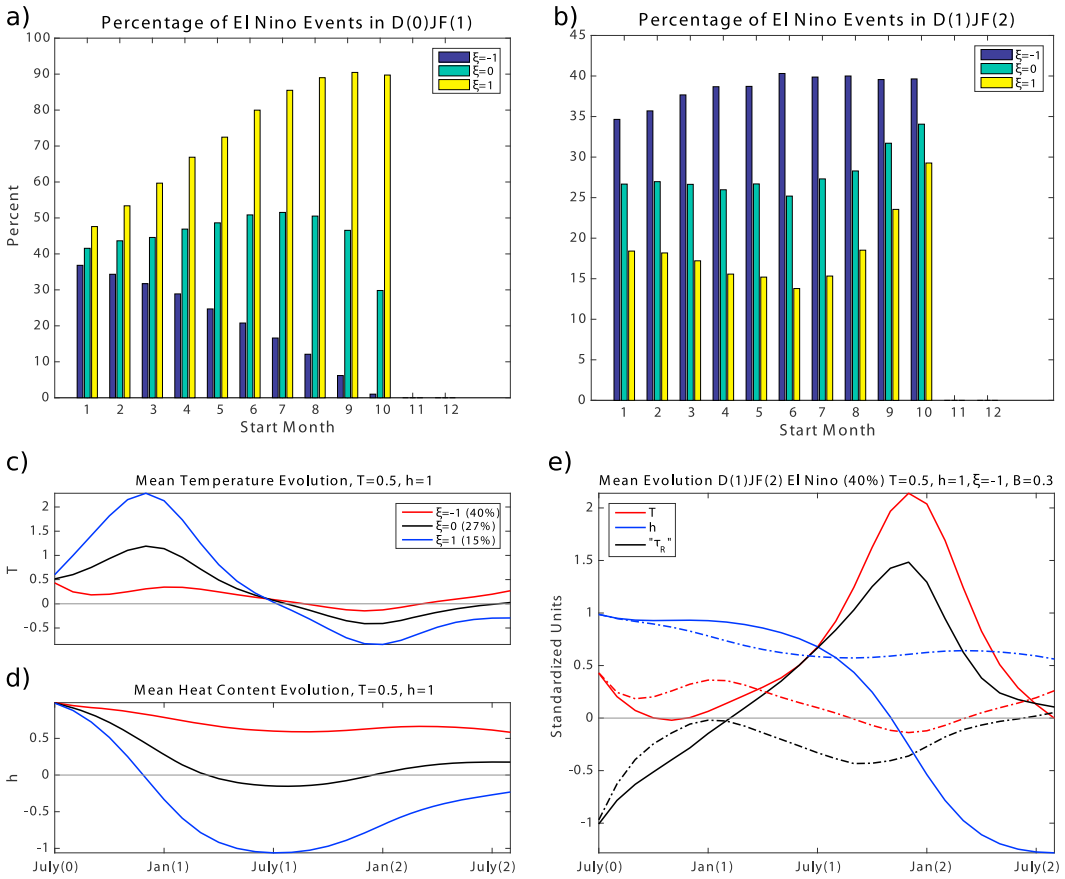

Figure 5. Results from 10,000 member ensembles using the conceptual model. (a) Percentage of El Niño events ($\bar{T} > 0.75$) that occur in the first winter (D(0)JF(1)) of the simulation by start month from the initial condition of $T = 0.5$, $h = 1$, and $\xi = 1$ (WWB), $\xi = 0$ (neutral), or $\xi = -1$ (EWB). (b) Percentage of El Niño events ($\bar{T} > 0.75$) that occur in the second winter (D(1)JF(2)) of the simulation by start month in year 0 from the initial condition of $T = 0.5$, $h = 1$, and $\xi = 1$ (WWB), $\xi = 0$ (neutral), or $\xi = -1$ (EWB). When run for an extended period of time, the model produces El Niño events in approximately one quarter of the years. (c) The mean temperature and (d) mean heat content evolution for the ensembles begun in July with initial conditions of $T = 0.5$, $h = 1$, and $\xi = 1$ (WWB), $\xi = 0$ (neutral), or $\xi = -1$ (EWB). (e) Comparison mean evolutions of the 40% (solid) of the ensemble members started in July with initial conditions of $T = 0.5$, $h = 1$, and $\xi = -1$ that produce an El Niño event in the second winter of the simulation versus the mean of the rest of the ensemble members (dashed).

5. Conceptual Model

To test more rigorously the impact of the summer EWB on a growing El Niño event and its potential effect in the second winter after the EWB (~18 months later), we use a conceptual recharge oscillator model written in nondimensional form as

$$\frac{dT}{dt} = -\lambda T + \omega_E h + \sigma\xi(1 + BH(T)T) \tag{2}$$

$$\frac{dh}{dt} = -\omega_E T \tag{3}$$

$$\frac{d\xi}{dt} = r\xi + w(t) \tag{4}$$

where

$$\lambda = \lambda_1 + \lambda_2 \sin(\omega_A t) = 2 + 2.5\sin(\omega_A t) \tag{5}$$

where λ is the growth rate and $\omega_E = \frac{1}{4}$, the ENSO frequency, both in years^{-1}. ξ is Gaussianly distributed red noise with a 45 day decorrelation timescale calculated from white noise, $w(t)$. $\sigma = 4.3$ years^{-1} is the noise

frequency, chosen such that the standard deviation of T in an extended simulation is approximately equal to the Nino3.4 index. $B = 0.3$ is the magnitude of the state dependence of noise forcing on SST and H a Heaviside function [*Levine and Jin*, 2015]. The model is integrated using a time step of 1 day. Equation 5 shows the growth rate annual cycle to correctly simulate the seasonal phase locking of ENSO and ω_A is the annual cycle frequency [*Stein et al.*, 2010, 2014]. This model is the same model as used by *Levine and McPhaden* [2015] to study the predictability of ENSO and to demonstrate the importance of WWB timing for the development of El Niño events. Further, *Levine and McPhaden* [2015] showed that the seasonal cycle of noise forcing had a small effect on the temperature variance at these leads, so σ will remain a constant. The experiment uses a 10,000 member ensemble for each initial condition. We are defining an El Niño event as an ensemble member that has a DJF anomaly exceeding 0.75. The results with the conceptual model rely quantitatively but not qualitatively on the values of the constants and the definition of an El Niño event chosen.

In particular, here we take the initial conditions of $T = 0.5$ and $h = 1$ to represent the growing El Niño and subject them to different noise forcings to compare the effect of WWBs and EWBs on the system. The results are not qualitatively dependent on the initial conditions (supporting information Figure S11). When run for an extended period, the model has approximately a one in four chance of there being an El Niño event in any given year. Figure 5a shows the likelihood of producing an El Niño event in the first winter of the integration (D(0)JF(1)) from these initial conditions dependent on start month and whether a WWB ($\xi = 1$), EWB ($\xi = -1$), or no wind burst ($\xi = 0$) occurs. There is a dramatic and increasing impact of WWBs and EWBs through the boreal spring and summer. WWBs significantly increase the likelihood of an El Niño event occurring in the first winter, while EWBs act oppositely to reduce it. It should also be noted that neither event is purely deterministic. For instance, a June or July EWB reduces the likelihood of an El Niño occurring to about 20% as opposed to the approximately 45% without a wind burst, but the EWB does not eliminate possibility of the El Niño event occurring. An example of this can be seen in 2002, when a June EWB was followed by a extended period of westerly wind forcing and an El Niño event resulted (supporting information Figure S13). Figure 5b is the same as Figure 5a except for the second winter of the simulation (D(1)JF(2)). EWBs that occur on growing El Niño conditions increase the likelihood of an El Niño event occurring during the second winter, while WWBs decrease this likelihood (due to increasing the likelihood of an event in the first winter).

Focusing on the simulations that start during July, as representative of 2014, the mean evolution of the EWB cases retains its heat content through the first winter and temperature anomalies remain small (Figure 5c and 5d). This is in contrast to the neutral forcing case which produces a moderate El Niño event and discharges its heat content anomaly and the WWB case which produces a large El Niño event, discharges heat content overshooting neutral, and then produces a La Niña event. In the 40% of the EWB cases that produce an El Niño event in the second winter, the model has a longer period of negative wind stress forcing and more retained heat content through to the first winter (Figure 5e) consistent with the dynamics found in *McGregor et al.* [2015]. With the ramping up of noise forcing during the second year, the chances of an extreme El Niño event also increase. The conceptual model captures the effect of the boreal summer easterly wind stress forcing on both temperature and WWV. Given the easterly wind burst that occurred in July 2014, the model suggests that not only is the likelihood of an El Niño reduced in the first winter [*Hu and Fedorov*, 2016] but there is also an increased likelihood of an El Niño event occurring during the second winter.

6. Conclusions

Here we have shown that not only did the EWB in summer of 2014 arrest the development of surface warming that year but it also halted the discharge of the anomalous WWV during 2014. In agreement with *McGregor et al.* [2015], episodic easterly wind stress forcing along the equator is a driving force for increases in WWV on the timescale of ~100 days, which we observe here as an increase in heat content in the months following the July 2014 EWB. Further, the remaining WWV generated from the early 2014 WWBs remained through the boreal winter of 2014-2015 giving a head start to the growth of the extreme El Niño of 2015–2016. This event is not unprecedented in the record, as 1990–1992 follows a similar pattern although the leftover WWV and later WWB forcing are weaker. This results in 1991–1992 being a moderate El Niño event as opposed to the extreme event observed in 2015-2016.

These results suggest that the time of year of the WWBs also plays a large role in determining the impact of the WWBs on the eventual development of an El Niño event. WWBs before the boreal spring can create conditions where through the boreal summer, it appears that an El Niño event is developing.

However, the subsequent episodic wind stress forcing still helps to determine the eventual outcome as to whether the El Niño event occurs and how strong the event eventually becomes. Overall, the impact of noise forcing on El Niño events drastically reduces the predictability of ENSO during the boreal summer months when ENSO is growing [*Zheng and Zhu*, 2010; *Levine and McPhaden*, 2015].

We find that just having a positive heat content anomaly is not enough to create an El Niño event [*Kessler*, 2002; *Philander and Fedorov*, 2003; *Zavala-Garay et al.*, 2004]. Heat content anomalies can remain in place for an extended duration before an El Niño event is triggered [*McGregor et al.*, 2015] and El Niño events require more than a single WWB to fully release the available energy stored in the anomalous WWV. Even after El Niño has begun to grow and equatorial heat discharge has begun, the developing El Niño event is further affected by subsequent wind stress forcing.

In both 1990 and 2014, a boreal summer EWB occurred halted the growth the of the incipient El Niño event and reversed the discharge of equatorial heat content. The increased equatorial heat content remained through the following winter giving a head start to the El Niño events of 1991 and 2015. In 2015, in particular, the heat content that remained from the false start of the 2014 El Niño event combined with the recharging that occurred following the boreal summer 2014 EWB, to create the fourth largest FMA WWV anomaly in the instrumental era. This elevated WWV anomaly, combined with strong WWBs in spring and summer of 2015—an example of state-dependent noise forcing favored by lingering warm SSTs at then end of 2014, resulted in the extreme El Niño event of 2015–2016.

Acknowledgments
This research was performed while the first author held a National Research Council Research Associateship Award at NOAA/PMEL. The authors would like to thank two anonymous reviewers for their helpful comments. This is PMEL contribution 4444. GODAS data provided by the NOAA/OAR/ESRL PSD, Boulder, Colorado, USA, from their Web site at http://www.esrl.noaa.gov/psd/. The TropFlux data is produced under a collaboration between Laboratoire d?Océanographie: Expérimentation et Approches Numériques (LOCEAN) from Institut Pierre Simon Laplace (IPSL, Paris, France) and National Institute of Oceanography/CSIR (NIO, Goa, India) and supported by Institut de Recherche pour le Développement (IRD, France). TropFlux relies on data provided by the ECMWF Re-Analysis Interim (ERA-I) and ISCCP projects. TropFlux is available at http://www.incois.gov.in/tropflux/.

References

Eisenman, I., L. Yu, and E. Tziperman (2005), Westerly wind bursts: ENSO's tail rather than the dog?, *J. Clim.*, *18*, 5224–5238.
Fedorov, A. V., S. Hu, M. Lengaigne, and E. Guilyardi (2014), The impact of westerly wind bursts and ocean initial state on the development, and diversity of El Niño events, *Clim. Dyn.*, *44*(5–6), 1381–1401, doi:10.1007/s00382-014-2126-4.
Hu, S., and A. V. Fedorov (2016), Exceptionally strong easterly wind burst stalling El Niño of 2014, *Proc. Natl. Acad. Sci.*, *113*(8), 2005–2010.
Hu, S., A. V. Fedorov, M. Lengaigne, and E. Guilyardi (2014), The impact of westerly wind bursts on the diversity and predictability of El Niño events: An ocean energetics perspective, *Geophys. Res. Lett.*, *41*(13), 4654–4663.
Ji, M., A. Leetmaa, and J. Derber (1995), An ocean analysis system for seasonal to interannual climate studies, *Mon. Weather Rev.*, *123*(2), 460–481.
Jin, F. F. (1997), An equatorial ocean recharge paradigm for ENSO. Part I: Conceptual model, *J. Atmos. Sci.*, *54*, 811–829.
Jin, F. F., L. Lin, A. Timmermann, and J. Zhao (2007), Ensemble-mean dynamics of the ENSO recharge oscillator under state dependent stochastic forcing, *Geophys. Res. Lett.*, *34*, L03807, doi:10.1029/2006GL027372.
Kessler, W. S. (2002), Is ENSO a cycle or a series of events?, *Geophys. Res. Lett.*, *29*(23), 2125, doi:10.1029/2002GL015924.
Kumar, B. P., J. Vialard, M. Lengaigne, V. Murty, and M. McPhaden (2012), TropFlux: Air-sea fluxes for the global tropical oceans-description and evaluation, *Clim. Dyn.*, *38*(7–8), 1521–1543.
Levine, A. F., and M. J. McPhaden (2015), The annual cycle in ENSO growth rate as a cause of the spring predictability barrier, *Geophys. Res. Lett.*, *42*, 5034–5041, doi:10.1002/2015GL064309.
Levine, A. F. Z., and F. F. Jin (2010), Noise-induced instability in the ENSO recharge oscillator, *J. Atmos. Sci.*, *67*, 529–542.
Levine, A. F. Z., and F. F. Jin (2015), A systematic approach to understanding the noise-ENSO interaction. Part I: A method for estimating the state-dependence of noise, *Clim. Dyn.*, doi:10.1007/s00382-015-2748-1.
McGregor, S., A. Timmermann, F.-F. Jin, and W. S. Kessler (2015), Charging El Niño with off-equatorial westerly wind events, *Clim. Dyn.*,1–18, doi:10.1007/s00382-015-2891-8.
McPhaden, M. J. (1999), Genesis and evolution of the 1997–98 El Niño, *Science*, *283*, 950–954.
McPhaden, M. J. (2002), Mixed layer temperature balance on intraseasonal timescales in the Equatorial Pacific Ocean, *J. Clim.*, *15*(18), 2632–2647.
McPhaden, M. J. (2012), A 21st century shift in the relationship between ENSO SST and warm water volume anomalies, *Geophys. Res. Lett.*, *39*, L09706, doi:10.1029/2012GL051826.
McPhaden, M. J. (2015), Playing hide and seek with El Niño, *Nat. Clim. Change*, *5*, 791–795.
McPhaden, M. J., H. P. Freitag, S. P. Hayes, B. A. Taft, Z. Chen, and K. Wyrtki (1988), The response of the equatorial Pacific Ocean to a westerly wind burst in May 1986, *J. Geophys. Res.*, *93*(C9), 10,589–10,603.
Meinen, C. S., and M. J. McPhaden (2000), Observations of warm water volume changes in the equatorial Pacific and their relationship to El Niño and La Niña, *J. Clim.*, *13*(20), 3551–3559.
Menkes, C. E., M. Lengaigne, J. Vialard, M. Puy, P. Marchesiello, S. Cravatte, and G. Cambon (2014), About the role of Westerly Wind Events in the possible development of an El Niño in 2014, *Geophys. Res. Lett.*, *41*, 6476–6483, doi:10.1002/2014GL061186.
Penland, C. (1996), A stochastic model of IndoPacific sea surface temperature anomalies, *Phys. D*, *98*, 534–558.
Penland, C., and P. D. Sardeshmukh (1995), The optimal growth of tropical sea surface temperature anomalies, *J. Clim.*, *8*, 1999–2024.
Philander, S. G., and A. Fedorov (2003), Is El Niño sporadic or cyclic?, *Annu. Rev. Earth Planet. Sci.*, *31*(1), 579–594.
Ren, H.-L., and F.-F. Jin (2013), Recharge oscillator mechanisms in two types of ENSO, *J. Clim.*, *26*(17), 6506–6523.
Smith, N. R. (1995), The BMRC ocean thermal analysis system, *Aust. Met. Mag*, *44*, 93–110.
Stein, K., N. Schneider, A. Timmermann, and F.-F. Jin (2010), Seasonal synchronization of ENSO events in a linear stochastic model, *J. Clim.*, *23*(21), 5629–5643.
Stein, K., A. Timmermann, N. Schneider, F.-F. Jin, and M. F. Stuecker (2014), ENSO seasonal synchronization theory, *J. Clim.*, *27*(2014), 5285–5310.
Stuecker, M. F., A. Timmermann, F. F. Jin, S. McGregor, and H. Ren (2013), A combination mode of the annual cycle and the El Niño/Southern Oscillation, *Nat. Geosci.*, *6*(2014), 540–544.

Wyrtki, K. (1985), Water displacements in the Pacific and the genesis of El Niño cycles, *J. Geophys. Res.*, *90*(C4), 7129–7132.
Yu, J.-Y., and H.-Y. Kao (2007), Decadal changes of ENSO persistence barrier in SST and ocean heat content indices: 1958–2001, *J. Geophys. Res.*, *112*, D13106, doi:10.1029/2006JD007654.
Yu, L., R. A. Weller, and T. W. Liu (2003), Case analysis of a role of ENSO in regulating the generation of westerly wind bursts in the western equatorial Pacific, *J. Geophys. Res.*, *108*(C4), 3128, doi:10.1029/2002JC001498.
Zavala-Garay, J., A. M. Moore, and R. Kleeman (2004), Influence of stochastic forcing on ENSO prediction, *J. Geophys. Res.*, *109*, C1107, doi:10.1029/2004JC002406.
Zheng, F., and J. Zhu (2010), Coupled assimilation for an intermediated coupled ENSO prediction model, *Ocean Dyn.*, *60*(5), 1061–1073.